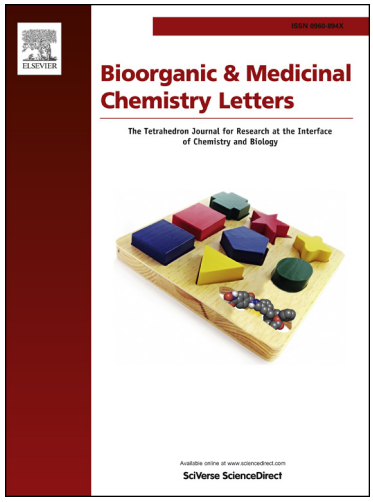

Design, synthesis and biological evaluation of pyrazolyl-nitroimidazole derivatives as potential EGFR/HER-2 kinase inhibitors

Xiang-Xiang Tao, Yong-Tao Duan, Long-Wang Chen, Dan-Jie Tang, Meng-Ru Yang, Peng-Fei Wang, Chen Xu, Hai-Liang Zhu

PII: S0960-894X(15)30248-1
DOI: http://dx.doi.org/10.1016/j.bmcl.2015.11.040
Reference: BMCL 23296

To appear in: *Bioorganic & Medicinal Chemistry Letters*

Received Date: 27 June 2015
Revised Date: 31 October 2015
Accepted Date: 13 November 2015

Please cite this article as: Tao, X-X., Duan, Y-T., Chen, L-W., Tang, D-J., Yang, M-R., Wang, P-F., Xu, C., Zhu, H-L., Design, synthesis and biological evaluation of pyrazolyl-nitroimidazole derivatives as potential EGFR/HER-2 kinase inhibitors, *Bioorganic & Medicinal Chemistry Letters* (2015), doi: http://dx.doi.org/10.1016/j.bmcl.2015.11.040

Design, synthesis and biological evaluation of pyrazolyl-nitroimidazole derivatives as potential EGFR/HER-2 kinase inhibitors

Xiang-Xiang Tao†, Yong-Tao Duan†, Long-Wang Chen†, Dan-Jie Tang, Meng-Ru Yang, Peng-Fei Wang, Chen Xu*, Hai-Liang Zhu*

State Key Laboratory of Pharmaceutical Biotechnology, Nanjing University, 163 Xianlin Road, Nanjing 210023, People's Republic of China

*Corresponding author. Tel. & fax: +86-25-89682572; e-mail: zhuhl@nju.edu.cn

†These three authors equally contributed to this paper.

Abstract

A series of novel pyrazole-nitroimidazole derivatives had been arranged and evaluated for their EGFR/HER-2 tyrosine kinase inhibitory activity as well as their antiproliferative properties on four kinds of cancer cell lines (MCF-7, Hela, HepG2, B16-F10). The bioassay results showed most of the designed compounds exhibited potential antiproliferation activity, with the IC_{50} values ranging from 0.13 μM to 128.06 μM in four tumor cell lines. Among them, compound **5c** exhibited remarkable inhibitory activity against EGFR/HER-2 tyrosine kinase with IC_{50} value of 0.26 μM / 0.51 μM respectively, comparable to the positive control erlotinib (IC_{50} = 0.41 μM for HER-2 and IC_{50} = 0.20 μM for EGFR) and lapatinib (IC_{50} = 0.54 μM for HER-2 and IC_{50} = 0.28 μM for EGFR). Molecular modeling simulation studies were performed in order to predict the biological activity of the proposed compounds and activity relationship (SAR) of these pyrazole-nitroimidazole derivatives.

Keywords:

Pyrazole-nitroimidazole derivatives

EGFR/HER-2 inhibitors

Anticancer activity

Cytotoxicity

Molecular docking and QSAR

The epidermal growth factor receptor (EGFR) and the homologous HER-2/ErbB-2 kinases, which are members of the type 1 or ErbB/HER receptor tyrosine kinase (RTK) family and closely implicated in cell proliferation, survival, adhesion, migration and differentiation,[1] have emerged as the most viable anticancer molecular targets in this family of four members, the others being HER-3 and HER-4.[2,3] The over expression or activating mutation of EGFR and/or HER-2 have always been observed in breast, ovarian, and non-small cell lung cancers[4,5,6] making them attractive therapeutic targets in cancers treatment.[7] EGFR and HER-2 are the hottest targets in current research and their over expression or abnormal activation often cause cell malignant transformation.[8] Also they have relationship with postoperative adverse, radiotherapy and chemotherapy resistance and tumor angiogenesis.[9] The blockade of EGFR and ErbB-2 has been clinically validated as an attractive approach for cancer therapy.[10,11]

In previous study, metronidazole/secnidazole (**Figure 1**), kinds of nitroimidazole, have been studied extensively for use as radiosensitizers due to their affinity for hypoxic tumors and molecular markers of hypoxic regions in solid tumors.[12] As we know, 2-Nitroimidazole derivatives, such as misonidazole and etanidazole, have been reported to have potent radiosensitising ability.[13,14] On the mechanism level, nitroimidazole derivatives attracted considerable attention as they showed a tendency to penetrate and accumulate in regions of tumors,[15,16] and were capable of undergoing bioreduction to yield electrophilic substances which can damage protein and nucleic acids. Our previous investigations have provided evidence of the antitumour properties of nitroimidazole ester derivatives and compound **a** (**Figure 1**) showed perfect antitumour activity with IC_{50} value of 0.62 μM for EGFR and 2.15 μM for HER-2.[17]

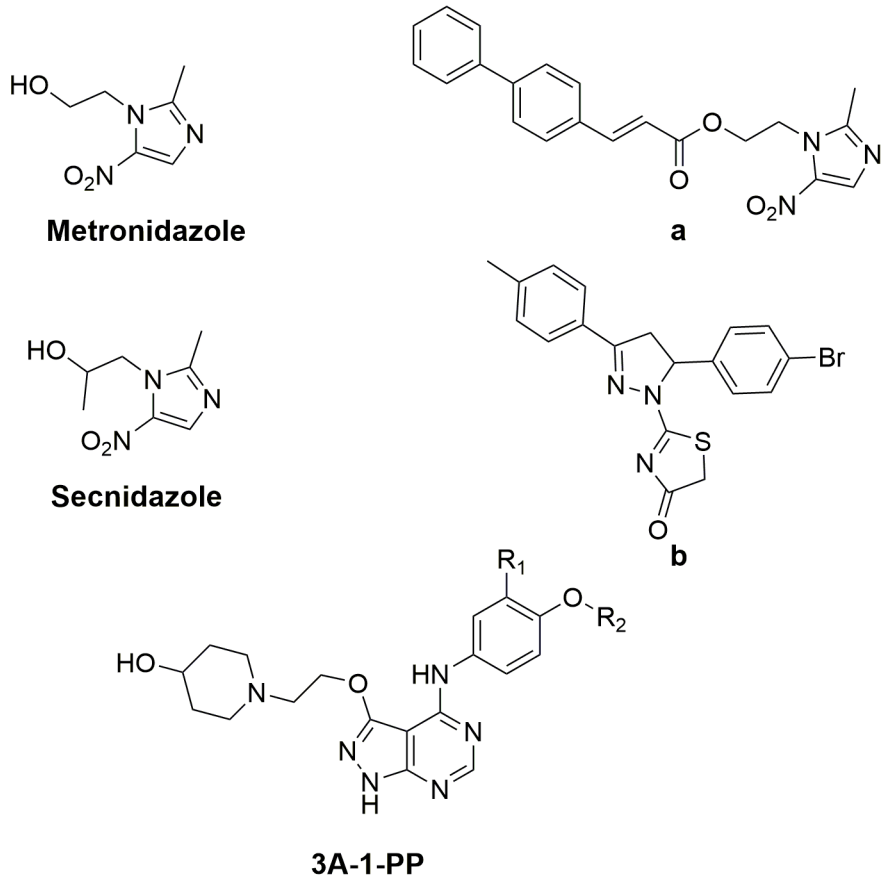

Figure 1. Chemical structures of some reported compounds

Also, pyrazolines have various activities and have versatile use in medicinal chemistry, it has been reported that anticancer compounds such as celecoxib, SC-5584, which have 4,5-dihydropyrazoles, the core structure of numerous biologically active compounds, always possess a wide range of bioactivities (anti-viral/anti-tumor,[18,19,20] antibacterial,[21,22] anti-inflammatory,[23] analgesic,[24] fungistatic,[25] and anti-hyperglycemic activity[26]). According to Richard Ducray et al. , 3 - alkoxy - 1H - pyrazolo [3, 4 - d] pyrimidines analogues (**3A - 1 - PP**) (**Figure 1**) showed potent EGFR and HER-2 receptor tyrosine kinase inhibitory activity, with IC_{50} values superior to positive control drug.[27] Besides, a series of novel compounds (for example: compound **b**) (**Figure 1**) containing the pyrazole motifs were reported as potent anticancer agents targeting EGFR tyrosine kinase and some of them had demonstrated potent anticancer activity.[28]

So far few reports have been dedicated to design and synthesize any anticancer/antitumor compound containing pyrazole and nitroimidazole. Herein, we describe the synthesis and structure-activity relationship (SAR) of a series of pyrazole derivatives containing nitroimidazole group, and present their *in vitro* antitumour activity and enzyme inhibition activity. Docking simulations are performed using the X-ray crystallographic structure of the EGFR in complex with an inhibitor to explore the binding modes of these compounds at the active site.

A series of novel pyrazole-nitroimidazole derivatives (**Table 1**) were synthesized by the routes outlined in **Scheme 1**. Compounds **3a - j** were synthesized through the reactions of 4-formylbenzoic acid with substituted acetophenone **2a - j** in ethanol by adding rapidly a stirred solution of NaOH in H_2O at room temperature. Synthesized compounds **3a - j** were treated with hydrazine hydrate in CH_3COOH which led to the formation of compounds **4a - j**. The synthesis of compounds **5a - j / 6a - j** was performed by reactions of the obtained compounds **4a - j** in the presence of metronidazole / secnidazole using EDC and DMAP as catalyst in CH_2Cl_2. The refined compounds were finally obtained by subsequent purification with chromatography. All of the target compounds gave satisfactory NMR data and analytical data, which in accordance with their designed structures.

Table 1. Chemical structures of pyrazolyl-nitroimidazole derivatives

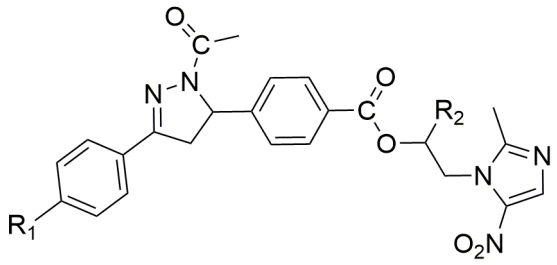

Compounds	R^1	R^2	Compounds	R^1	R^2
5a	H	H	**5f**	OCH_2CH_3	H
6a	H	CH_3	**6f**	OCH_2CH_3	CH_3
5b	Br	H	**5g**	Cl	H
6b	Br	CH_3	**6g**	Cl	CH_3

5c	CF_3	H	**5h**	F	H
6c	CF_3	CH_3	**6h**	F	CH_3
5d	OCH_3	H	**5i**	I	H
6d	OCH_3	CH_3	**6i**	I	CH_3
5e	NO_2	H	**5j**	CH_3	H
6e	NO_2	CH_3	**6j**	CH_3	CH_3

Scheme 1[a].

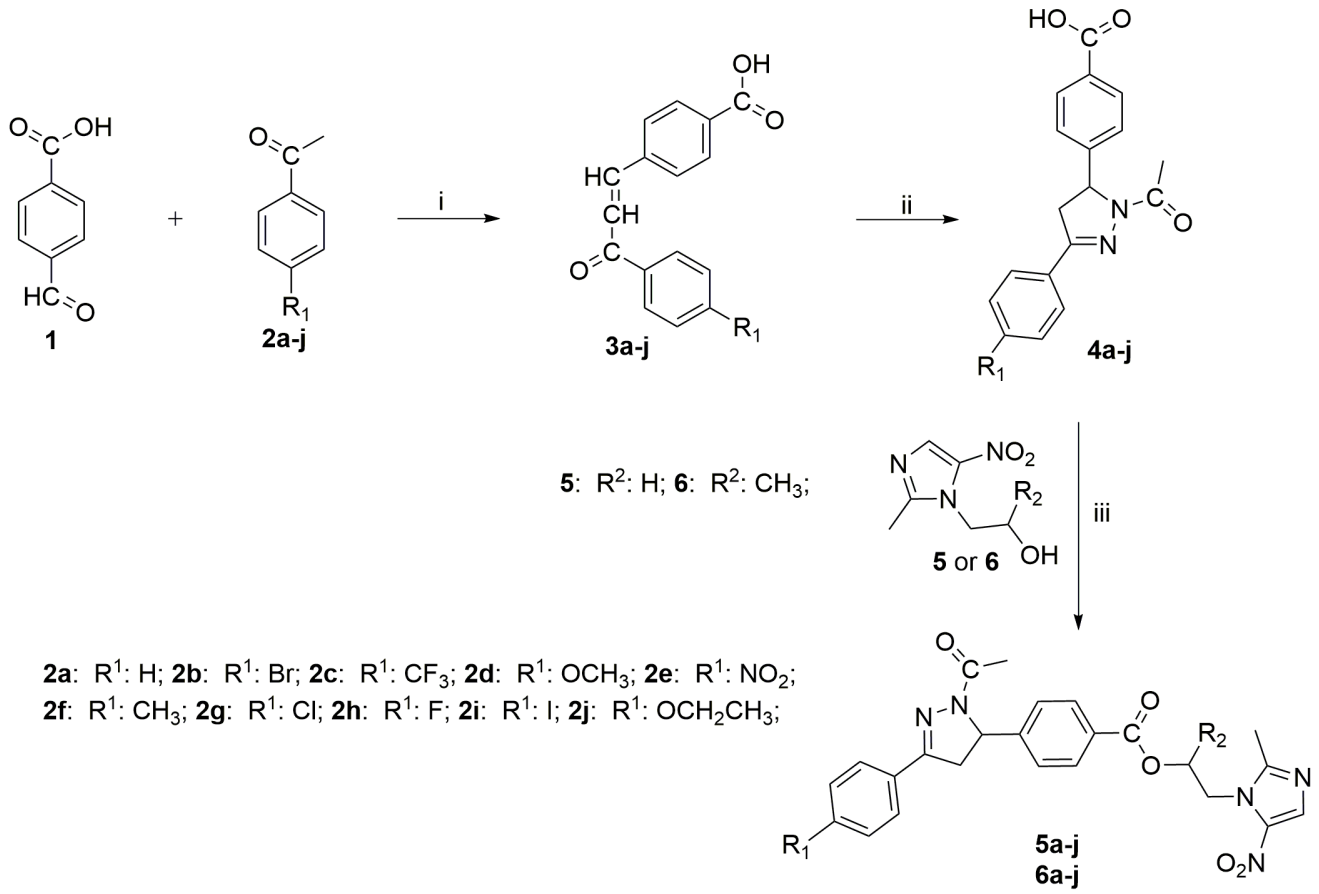

[a]**Reagents and conditions**: (i) Ethanol, NaOH / H_2O=1:10, RT, 8h; (ii) CH_3COOH, Hydrazine Hydrate, reflux, 12h; (iii) CH_2Cl_2, EDC, DMAP, reflux,12 h.

Four cultured cancer cell lines: human hepatoma cells (HepG2), human breast cancer cells (MCF-7), human cervical cancer cell line (Hela) as well as mouse melanoma cells (B16-F10) were exploited in the anticancer assay. The test followed the MTT assay and used erlotinib and lapatinib under identical conditions as control. The IC_{50} of the compounds against these cancer cells were presented in **Table 2**. Results revealed that

some synthesized compounds exhibited potential antiproliferative activities, with the most promising IC_{50} 0.13 μM.

Table 2. *In vitro* anticancer activities (IC_{50}, μM [a]) of all compounds against tumor cell lines

Compounds	R^1	R^2	IC_{50} (μM [a] ± SD)	IC_{50} (μM [a] ± SD)	IC_{50} (μM [a] ± SD)	IC_{50} (μM [a] ± SD)
			Hela [b]	MCF-7 [b]	HepG2 [b]	B16-F10 [b]
5a	H	H	48.82±0.17	58.21±1.67	42.21±4.12	62.73±3.11
6a	H	CH_3	45.21±1.18	49.92±0.89	43.81±1.91	68.24±2.16
5b	Br	H	2.82±0.08	5.56±0.13	3.82±0.27	13.09±0.07
6b	Br	CH_3	11.78±0.14	8.92±0.36	9.02±0.12	10.76±0.20
5c	CF_3	H	0.13±0.05	0.96±0.13	0.33±0.16	0.19±0.08
6c	CF_3	CH_3	0.42±0.02	2.18±0.08	2.21±0.08	5.87±0.14
5d	OCH_3	H	27.87±0.17	30.20±0.26	15.81±0.15	36.21±0.52
6d	OCH_3	CH_3	35.13±1.15	27.98±0.56	25.21±0.79	40.58±0.62
5e	NO_2	H	0.15±0.10	1.13±0.07	1.75±0.23	0.38±0.12
6e	NO_2	CH_3	3.78±0.27	3.33±0.56	3.62±0.55	12.22±0.13
5f	OCH_2CH_3	H	31.35±0.41	20.62±0.56	19.28±0.40	38.91±1.17
6f	OCH_2CH_3	CH_3	47.65±1.23	40.62±1.72	38.82±0.89	46.56±1.12
5g	Cl	H	4.13±0.07	2.27±0.11	3.31±0.12	4.82±0.25
6g	Cl	CH_3	15.62±0.17	8.82±0.27	12.20±0.17	22.19±0.18
5h	F	H	2.45±0.11	1.67±0.05	1.89±0.03	4.19±0.10
6h	F	CH_3	7.42±0.51	5.21±0.21	8.89±0.21	15.52±0.10
5i	I	H	7.53±0.21	4.85±0.17	6.28±0.09	11.77±0.22
6i	I	CH_3	25.62±0.72	9.77±0.23	9.98±0.21	19.13±0.08
5j	CH_3	H	76.77±1.21	70.65±7.78	50.16±1.77	>100
6j	CH_3	CH_3	72.12±1.45	92.12±0.89	58.12±1.82	>100
Erlotinib			0.20±0.06	0.10±0.01	0.12±0.05	0.17±0.08
Lapatinib			0.12±0.02	0.47±0.03	0.27±0.06	0.21±0.03

[a]Antiproliferation activity was measured using the MTT assay. Values are the average of six independent experiments run in triplicate. Variation was generally 5-10%.

[b]Cancer cells kindly supplied by State Key Laboratory of Pharmaceutical Biotechnology, Nanjing University.

On the whole, these compounds exhibit stronger anticancer activities against Hela and HepG2 cell lines. Against Hela, compounds **5e** (IC_{50} = 0.15 μM)**, 6c** (IC_{50} = 0.42 μM) are comparable to erlotinib (IC_{50} = 0.20 μM). Then against B16-F10, compounds **5e** (IC_{50} = 0.38 μM) are comparable to lapatinib (IC_{50} = 0.21 μM). Notably, compound **5c** showed broad-spectrum anticancer activity against all the four cell lines, with IC_{50} of 0.13 to 0.96

μM. These results suggested that compound **5c** is more potent than other compounds overall.

To enhance the antiproliferation activity against Hela or HepG2 cell lines, electron-withdrawing groups tended to be preferable to electron-donating groups for pyrazolyl-nitroimidazole derivatives. This conclusion is especially true when substituent R^2 comes to be constant and substituent R^1 varies simultaneously, because the order of electron-withdrawing potential is: trifluoromethyl > halogen > hydrogen > methyl and the order of anticancer potential is: **5c** > **5h** > **5i** > **5a** > **5j**.

To further illustrate the effect of substituent R^2 on cell antiproliferation, we also carried out the control comparison by maintaining substituent R^1 unchanged. The results indicated that when substituent R^2 was hydrogen rather than methyl, anticancer activity of the compound always reached a favorable level. On account of diverse nitroimidazoles with alteration of substituent R^2, the massive disparities in value of IC_{50} existed between series **5 (5a - j)** and series **6 (6a - j)**. Comparison of mean value and the most potent value of IC_{50} of series **5 (5a - j)** or series **6 (6a - j)** against Hela and HepG2 cell lines implied that substituent R^2 determine the bioactivity of pyrazolyl-nitroimidazole derivatives to a great extent.

To test whether the inhibition of cell growth of Hela was related to cell apoptosis, Hela cell apoptosis induced by compound **5c** was determined using flow cytometry. The uptake of Annexin V-PE was significantly increased, and the uptake of normal cells was significantly decreased in a density-dependent manner. Finally the percentage of total apoptotic cells was markedly elevated in a dose-dependent manner from 24.22% to 80.9% at 48 h. As shown in **Figure 2**, we treated Hela cells with different doses of **5c** and found that the 0.13 μM-treated group displayed double apoptosis than control-treated group. Meanwhile, we compare apoptosis of 0.26 μM-, 0.52μM-, and 1.04 μM-treated groups with that of 0.13 μM-treated group, then drew the conclusion that the percentage of apoptotic cell significantly increased after treatment with high doses of **5c**.

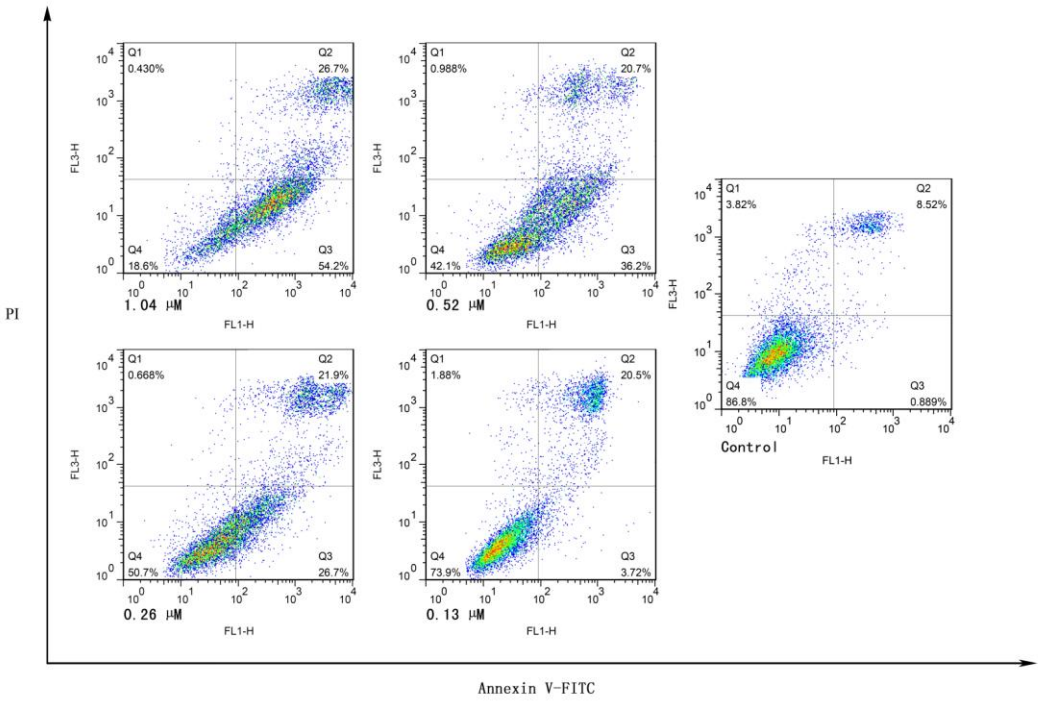

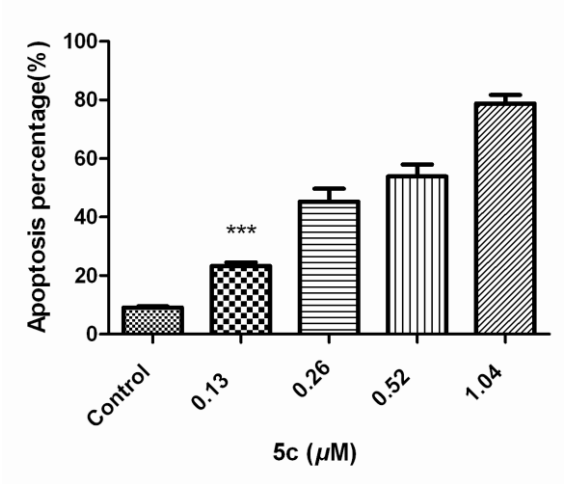

Figure 2. Hela cells treated with 0.13, 0.26, 0.52 and 1.04 μM **5c** for 48 hours were collected and processed for analysis. The percentage of early apoptotic cells in the lower right quadrant (annexin V-FITC positive/PI negative cells), as well as late apoptotic cells located in the upper right quadrant (annexin V-FITC positive/PI positive cells). Images were representative of three independent experiments. Data were mean ± S.E.M. of three independent experiments. Values represent the mean, n = 3. $^{***}P < 0.001$.

All compounds were evaluated for their abilities to inhibit the auto-phosphorylation of EGFR and HER-2 kinases using a solid-phase activity-test kit. The inhibition constants (IC_{50}) of the compounds were summarized in **Table 3**. For the given compounds, it was observed that the IC_{50} value for inhibition of EGFR kinase was higher than that observed of HER-2 kinase. Obviously, they had the same trends. It was evident that there is also a reasonable correlation between the EGFR and HER-2 inhibitory activities; thus, this was not surprising in view of the high sequence homology of the catalytic domains of these two kinases. As shown in **Table 3**, among the tested compounds, compound **5c** showed potent anticancer activity with IC_{50} of 0.26 and 0.51 μM against EGFR and HER-2 respectively, which were comparable to the positive control erlotinib (IC_{50} = 0.41 μM for HER-2 and IC_{50} = 0.20 μM for EGFR) and lapatinib (IC_{50} = 0.54 μM for HER-2 and IC_{50} = 0.28 μM for EGFR). Other tested compounds displayed moderate inhibitory activities with IC_{50} ranging from 0.60 to 25.58 μM. The results of EGFR and HER-2 kinases inhibitory activity of the tested compounds correlated with the structural relationships (SAR) of their inhibitory effects on the cell proliferation assay. This suggests that the potent inhibitory effects of the synthetic compounds on the cell proliferation assay were causally related to their kinase inhibitory activities.

Table 3. Inhibition activities of all compounds against EGFR and HER-2

Compounds	IC_{50} ($\mu M^a \pm SD$)	IC_{50} ($\mu M^a \pm SD$)
	EGFR	HER-2
5a	9.58±0.24	14.04±1.12
6a	12.24±1.13	17.00±10.77
5b	4.13±0.20	3.45±0.25
6b	5.96±0.82	8.27±1.01
5c	0.26±0.03	0.51±0.06
6c	6.67±0.11	5.62±0.33
5d	8.54±0.55	17.25±1.63
6d	21.31±0.52	12.05±6.33
5e	0.60±0.02	2.06±0.09
6e	1.45±0.06	3.53±0.08
5f	15.16±2.86	14.93±1.02

6f	26.92±1.58	18.12±2.69
5g	7.37±0.56	4.10±0.89
6g	9.26±0.56	9.96±1.12
5h	5.02±0.33	4.07±1.01
6h	6.58±0.73	8.54±0.63
5i	1.26±0.15	2.75±0.24
6i	10.69±1.02	12.66±2.54
5j	10.92±1.11	13.16±1.46
6j	25.58±1.09	18.89±2.11
Erlotinib	0.20±0.02	0.41±0.02
Lapatinib	0.28±0.03	0.54±0.02

[a]EGFR/HER-2 inhibitory activity was measured using the MTT assay. Values are the average of six independent experiments run in triplicate. Variation was generally 5-10%.

Six compounds selected on the basis of their antiproliferative activity were evaluated for their toxicity against human kidney epithelial cell 293T with the median cytotoxic concentration (CC_{50}) data of tested compounds by the MTT assay. These compounds were tested at multiple doses to assess the viability of 293T. As shown in **Table 4**, six compounds were selected on the basis of their potent IC_{50} values against EGFR/HER-2 tyrosine kinase and tumor cell lines. Judging from the median cytotoxic concentration (CC_{50}) data, it demonstrated that the compounds selected according to their anticancer activity exhibit hypotoxicity in vitro against human kidney epithelial cell 293T.

Table 4. The median cytotoxic concentration (CC_{50}) data of tested compounds

Compounds	CC_{50}, μM[a]	**Compounds**	CC_{50}, μM[a]
5c	98.86	**5g**	137.91
5e	78.83	**6e**	168.27
5h	117.52	**Erlotinib**	104.76
6c	92.60	**Lapatinib**	123.17

[a]The cytotoxicity of each compound was expressed as the concentration of compound that reduced cell viability to 50% (CC_{50}).

In order to gain better understanding on the potency of the 20 compounds and guide further SAR studies, we proceeded to examine the interaction of these compounds with

EGFR (PDB code: 1M17) by molecular docking, which was performed by simulation of the 20 compounds into the ATP binding site in EGFR. All docking runs were applied the Lamarckian genetic algorithm of Auto-Dock 3.5. The obtained results were presented in **Figure 3** and **Figure 4(b)**, which showed the optimal binding mode of compound **5c** interacting with the 1M17 protein. The amino acid residues which had interaction with EGFR were labeled. In the binding mode, compound **5c** was nicely bound to EGFR via three charge interactions, one π-cation interaction, one hydrogen bond interaction and one Van der Waals interaction. Lys721 formed one π-cation interaction with imidazole ring and one charge interaction with oxygen atom of nitro group on imidazole ring. And more, two charge interactions were found between Asp831, Glu738 and nitrogen atom of nitro group on imidazole ring. Meanwhile, a Van der Waals interaction was formed between oxygen atom of carbonyl group on pyrazole ring and Cys773. At last, one hydrogen bond interaction displayed in presence of Lys692 and fluoride atom of trifluoromethyl group.

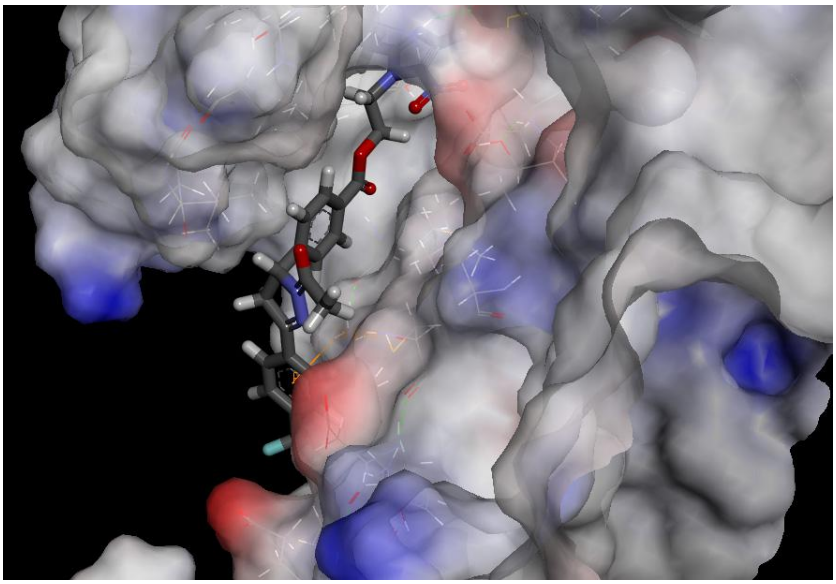

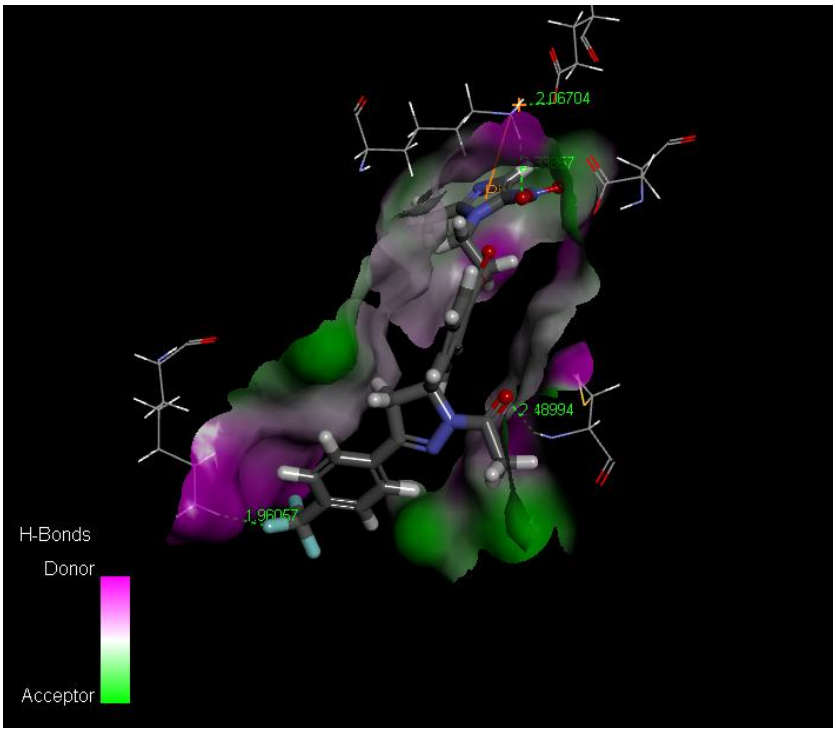

Figure 3. Molecular docking 3D model of the interaction between compound **5c** and EGFR enzyme: for clarity, only interacting residues are displayed.

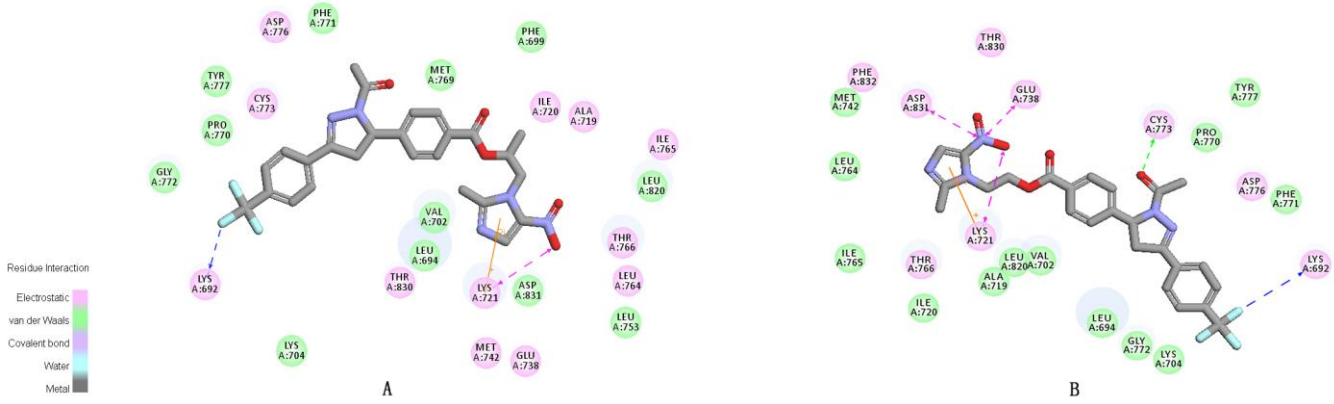

Figure 4. (**a**) Molecular docking 2D model of the interaction between compound **6c** and EGFR enzyme: for clarity, only interacting residues are displayed. (**b**) Molecular docking 2D model of the interaction between compound **5c** and EGFR enzyme: for clarity, only interacting residues are displayed.

In addition, the predicted binding interaction energy was used as the criterion for ranking; the estimated interaction energies of other synthesized compounds were ranging

from -53.05 to -43.30 kcal/mol, as displayed in **Figure 5** with histogram. The selected compound of **5c** had a best estimated binding free energy of -54.11 kcal/mol for EGFR. These molecular docking results, along with the biological assay data, suggested that compound **5c** is a potential inhibitor of EGFR.

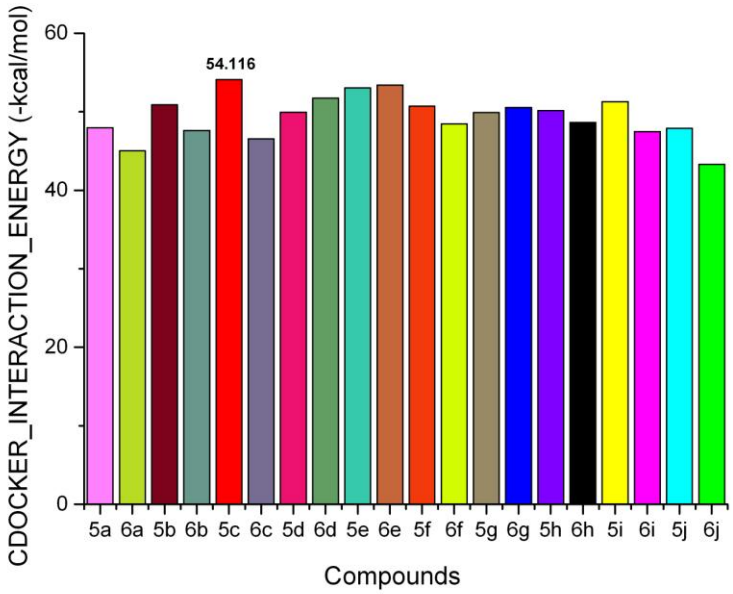

Figure 5. The histogram about CDOCKER_INTERACTION_ENERGY (-kcal/mol) of all compounds for EGFR

Besides, for further understanding the influence of substituent R^2 on bioactivity of compounds, we also compare molecular modeling result of compound **6c** with that of compound **5c**. As shown in **Figure 4(a),** in the binding mode of compound **6c** interacting with the 1M17 protein, compound **6c** was bound to EGFR via one charge interactions, one π-cation interaction, and one hydrogen bond interaction. Obviously, interactions between compounds **6c** and 1M17 protein decreased, which in accordance with the differences between compounds **5c** and **6c** in predicted binding interaction energy presented in **Figure 5**.

In order to acquire a systematic SAR profile on 20 compounds as antitumor agents and explore the more powerful EGFR inhibitors, 3D-QSAR model was built to choose activity conformation of the designed molecular and reasonably evaluated the designed

molecules by using the corresponding pIC_{50} values which were converted from the obtained IC_{50} (μM) values of EGFR inhibition and performed by built-in QSAR software of DS 3.5 (Discovery Studio 3.5, Accelrys, Co. Ltd). The way of this transformation was derived from an online calculator developed from an Indian clinical chemistry lab (http://www.sanjeevslab.org/tools-IC_{50}.html). The training and test set was divided by the random diverse molecules method of DS 3.5, in which the test set accounts for 25% while the training set was set to 75%. The training set composed 15 agents and 5 agents were consisted of the relative test set, which had been presented in **Table 5**. The success of this model depended on docking study and the reliability of previous study about activity data.

Table 5. The experimental and predicted inhibitory activity of all compounds by 3D-QSAR models based upon active conformation achieved by molecular docking

Compounds [a]	EGFR		Residual error
	Actual pIC_{50}	Predicted pIC_{50}	
5a	5.018	5.068	-0.050
5b	5.384	5.354	0.030
5c	6.521	6.487	0.034
5d	5.068	5.327	-0.259
5e	6.221	6.237	-0.016
5f	4.819	5.289	-0.470
5g	5.132	5.434	-0.302
5h	5.299	5.221	0.078
5i	5.899	5.761	0.138
5j	4.961	5.247	-0.286
6a	4.912	4.865	0.047
6b	5.224	4.941	0.283
6c	5.175	5.238	-0.063
6d	4.671	4.549	0.122
6e	5.838	5.819	0.019
6f	4.569	4.538	0.031
6g	5.033	5.039	-0.006
6h	5.181	5.065	0.116
6i	4.971	4.962	0.009
6j	4.592	4.758	-0.166

[a]The underlined for the test set, and the rest for training.

In default situation, the alignment conformation of each molecule that possessed the lowest CDOCKER_INTERACTION_ENENGY among the ten docked poses. The 3D-QSAR model generated from DS 3.5, defined the critical regions (steric or electrostatic) affecting the binding affinity. The graphical relationship of observed and predicted values had been illustrated in **Figure 6(c)**, in which the plot of the observed IC_{50} versus the predicted values showed that this model could be used in prediction of activity.

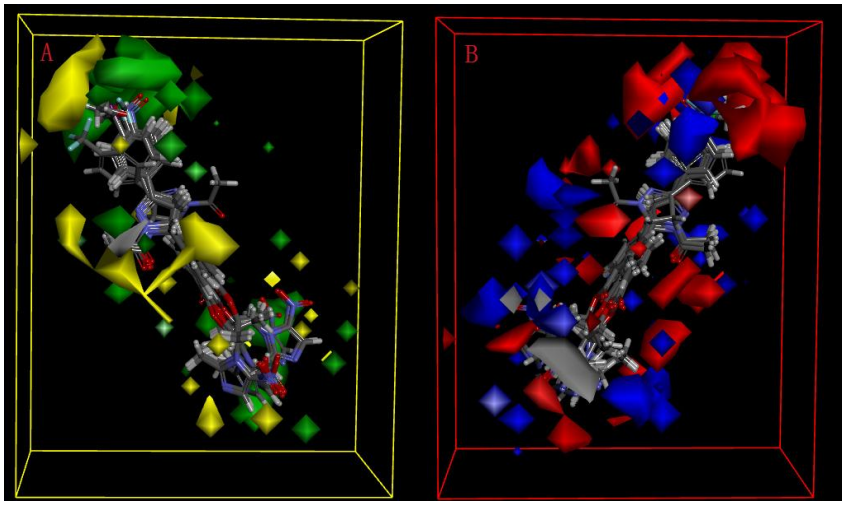

(a) & (b)

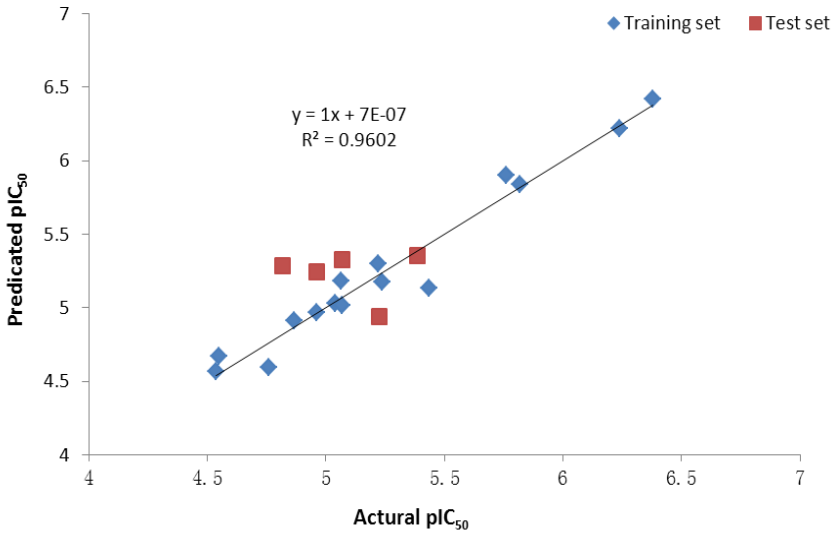

(c)

Figure 6. (**a**) Isosurface of the 3D-QSAR model coefficients on Van der Waals grids. The green triangle mesh representation indicates positive coefficients; the yellow triangle mesh indicates negative coefficients. (**b**) Isosurface of the 3D-QSAR model coefficients on electrostatic potential grids. The blue triangle mesh represents positive electrostatic potential and the red area represents negative electrostatic potential. (**c**) Using linear fitting curve to compare the predicted pIC_{50} value with that of experiment.

A contour plot of the electrostatic field region favorable (in blue) or unfavorable (red) for anticancer activity based on EGFR target were shown in **Figure 6(b)** while the energy grids corresponding to the favorable (in green) or unfavorable (yellow) steric effects for the EGFR affinity were shown in **Figure 6(a)**. It was widely acceptable that a better inhibitor based on the 3D-QSAR model should have strong Van der Waals attraction in the green areas and a polar group in the blue electrostatic potential areas (which were dominant close to the skeleton).

In summary, a series of pyrazole-nitroimidazole derivatives were synthesized and their biological ability was evaluated for EGFR/HER-2 tyrosine kinase inhibition as well as MTT assay *in vitro*. Results showed these compounds possessed potent antiproliferative activity against EGFR/HER-2 tyrosine kinase with IC_{50} values in microM range. Among them, the promising IC_{50} values of compound **5c** against EGFR/HER-2 tyrosine (0.26 μM / 0.51 μM) and human cervical cancer cell line (Hela) (0.13 μM) indicated that compound **5c** could be the potential EGFR/HER-2 tyrosine kinase inhibitor and anti-tumor agent. Docking simulation was carried out to find the probable binding models and poses by means of DS 3.5 (Discovery Studio 3.5, Accelrys, Co. Ltd). QSAR models facilitated us to validate the reasonable design of EGFR/HER-2 inhibitors in the future.

References and notes

1. Hynes, N. E.; Lane, H. A. *Nat. Rev. Cancer.* **2005,** *5*, 341.
2. Fantl, W. J.; Johnson, D. E.; Williams, L. T. *Annu. Rev. Biochem.* **1993,** *62*, 453.
3. Kamath, S.; Buolamwini, J. K. *J. Med. Chem.* **2003,** *46*, 4657.
4. Aaronson, S. A. *Science* **1991,** *254*, 1146.
5. Li, J.; Yen, C.; Liaw, D.; Podsypanina, K.; Bose, S.; Wang, S. I.; Puc, J.; Miliaresis, C.; Rodgers, L.; McCombie, R. *science* **1997,** *275*, 1943.
6. Marshall, C. *Cell* **1995,** *80*, 179.
7. De Bono, J. S.; Rowinsky, E. K. *Trends. Mol. Med.* **2002,** *8*, S19.
8. Cha, M. Y.; Lee, K.-O.; Kang, S.-J.; Jung, Y. H.; Song, J. Y.; Choi, K. J.; Byun, J. Y.; Lee, H.-J.; Lee, G. S.; Park, S. B. *J. Med. Chem.* **2012,** *55*, 2846.
9. Ciardiello, F.; Tortora, G. *Clin. Cancer. Res.* **2001,** *7*, 2958.
10. Li, D.-D.; Qin, Y.-J.; Sun, J.; Li, J.-R.; Fang, F.; Du, Q.-R.; Qian, Y.; Gong, H.-B.; Zhu, H.-L. *Plos One* **2013,** *8*, e69427.
11. Higa, G. M.; Abraham, J. *Expert. Rev. Anticanc.* **2007,** *7*, 1183.
12. Giglio, J.; Fernández, S.; Rey, A.; Cerecetto, H. *Bioorg. Med. Chem. Lett.* **2011,** *21*, 394.
13. Brown, J. M.; Ning, Y. Y.; Brown, D. M.; Lee, W. W. *Int. J. Radiat. Oncol.* **1981,** *7*, 695.
14. Walton, M. I.; Workman, P. *Biochem. Pharmacol.* **1987,** *36*, 887.
15. Born, J. L.; Smith, B. R.; Harper, N.; Koch, C. J. *Biochem. Pharmacol.* **1992,** *43*, 1337.
16. Mallia, M. B.; Subramanian, S.; Banerjee, S.; Sarma, H.; Venkatesh, M. *Bioorgan. Med. Chem.* **2006,** *14*, 7666.
17. Qian, Y.; Zhang, H.-J.; Zhang, H.; Xu, C.; Zhao, J.; Zhu, H.-L. *Bioorgan. Med. Chem.* **2010,** *18*, 4991.
18. Manfredini, S.; Bazzanini, R.; Baraldi, P. G.; Guarneri, M.; Simoni, D.; Marongiu, M. E.; Pani, A.; La Colla, P.; Tramontano, E. *J. Med. Chem.* **1992,** *35*, 917.
19. Manfredini, S.; Bazzanini, R.; Baraldi, P.; Bonora, M.; Marangoni, M.; Simoni, D.; Pani, A.; Scintu, F.; Pinna, E.; Pisano, L. *Anti-cancer. Drug. Des.* **1996,** *11*, 193.
20. Park, H.-J.; Lee, K.; Park, S.-J.; Ahn, B.; Lee, J.-C.; Cho, H.; Lee, K.-I. *Bioorg. Med. Chem. Lett.* **2005,** *15*, 3307.
21. Tanitame, A.; Oyamada, Y.; Ofuji, K.; Fujimoto, M.; Iwai, N.; Hiyama, Y.; Suzuki, K.; Ito, H.; Terauchi, H.; Kawasaki, M. *J. Med. Chem.* **2004,** *47*, 3693.
22. Kuecuekguezel, S. G.; Rollas, S.; Erdeniz, H.; Kiraz, M.; Ekinci, A. C.; Vidin, A. *Cheminform* **2000,** *31*,398.
23. Penning, T. D.; Talley, J. J.; Bertenshaw, S. R.; Carter, J. S.; Collins, P. W.; Docter, S.; Graneto, M. J.; Lee, L. F.; Malecha, J. W.; Miyashiro, J. M. *J. Med. Chem.* **1997,** *40*, 1347.
24. Menozzi, G.; Mosti, L.; Fossa, P.; Mattioli, F.; Ghia, M. *J. Heterocyclic. Chem.* **1997,** *34*, 963.
25. Sridhar, R.; Perumal, P. T.; Etti, S.; Shanmugam, G.; Ponnuswamy, M. N.; Prabavathy, V. R.; Mathivanan, N. *Bioorg. Med. Chem. Lett.* **2004,** *14*, 6035.
26. Bebernitz, G. R.; Argentieri, G.; Battle, B.; Brennan, C.; Balkan, B.; Burkey, B. F.; Eckhardt, M.; Gao, J.; Kapa, P.; Strohschein, R. J. *J. Med. Chem.* **2001,** *44*, 2601.
27. Ducray, R.; Ballard, P.; Barlaam, B. C.; Hickinson, M. D.; Kettle, J. G.; Ogilvie, D. J.; Trigwell, C. B. *Bioorg. Med. Chem. Lett.* **2008,** *18*, 959.

28. Qiu, K. M.; Wang, H. H.; Wang, L. M.; Luo, Y.; Yang, X. H.; Wang, X. M.; Zhu, H. L. *Bioorgan. Med. Chem.* **2012,** *20,* 2010.

Figure Captions

Table 1. Chemical structures of pyrazole-nitroimidazole derivatives.

Table 2. *In vitro* anticancer activities (IC_{50}, μM) of all compounds against tumor cell lines.

Table 3. Inhibition activities of all compounds against EGFR and HER-2.

Table 4. The median cytotoxic concentration (CC_{50}) data of tested compounds.

Table 5. The experimental and predicted inhibitory activity of all compounds by 3D-QSAR models based upon active conformation achieved by molecular docking

Figure 1. Chemical structures of some reported compounds.

Figure 2. Hela cells treated with 0.13, 0.26, 0.52 and 1.04 μM **5c** for 48 hours were collected and processed for analysis. The percentage of early apoptotic cells in the lower right quadrant (annexin V-FITC positive/PI negative cells), as well as late apoptotic cells located in the upper right quadrant (annexin V-FITC positive/PI positive cells). Images were representative of three independent experiments. Data were mean ± S.E.M. of three independent experiments. Values represent the mean, n =4. $^{***}P < 0.001$.

Figure 3. Molecular docking 3D model of the interaction between compound **5c** and EGFR enzyme: for clarity, only interacting residues are displayed.

Figure 4. (**a**) Molecular docking 2D model of the interaction between compound **6c** and EGFR enzyme: for clarity, only interacting residues are displayed. (**b**) Molecular docking 2D model of the interaction between compound **5c** and EGFR enzyme: for clarity, only interacting residues are displayed.

Figure 5. The histogram about CDOCKER_INTERACTION_ENERGY (-kcal/mol) of all compounds for EGFR

Figure 6. (**a**) Isosurface of the 3D-QSAR model coefficients on Van der Waals grids. The green triangle mesh representation indicates positive coefficients; the yellow triangle mesh indicates negative coefficients. (**b**) Isosurface of the 3D-QSAR model coefficients on electrostatic potential

grids. The blue triangle mesh represents positive electrostatic potential and the red area represents negative electrostatic potential. (**c**) Using linear fitting curve to compare the predicted pIC_{50} value with that of experiment.

Scheme 1[a]**.**

Graphical abstract